# Performance of p-Bulk Microstrip Sensors under $^{60}$Co $\gamma$ Irradiation at Rates Expected at the HL-LHC

Y. Takahashi[a], K. Hara[a,*], S. Kim[a], Y. Ikegami[b], Y. Takubo[b], S. Terada[b], Y. Unno[b], S. Mitsui[c], S. Kamada[d], K. Yamamura[d]

[a] *IPAS, University of Tsukuba, Tsukuba, Ibaraki 305-8571 Japan*
[b] *INPS, High Energy Accelerator Research Org. (KEK), Tsukuba, Ibaraki 305-0801 Japan*
[c] *Sokendai, 1-1- Oho, Tsukuba, Ibaraki 305-0801 Japan*
[d] *Hamamatsu Photonics Co. Ltd., Ichino, Hamamatsu Shizuoka 435-0051 Japan*

**Abstract**

We are developing p-bulk microstrip sensors for the high luminosity upgrade of the LHC accelerator, HL-LHC. The stability of FZ (float zone) wafers available to Hamamatsu Photonics was examined by irradiating them at rates expected at the HL-LHC. They show degradation in the operational voltage at low dose but recover after the dose is accumulated. The instability is dependent on the bias voltage and dose rate, and also on the irradiation history. We have characterized the instability and attributed the cause to the charge concentration at the electrode edge. The strip isolation, which is degraded while in irradiation, is shown not to induce any practical problem for the operation.

*Keywords:* HL-LHC, p-bulk, microstrip sensor, ionization dose, stability

## 1. Introduction

The Large-Hadron Collider (LHC) will undergo substantial upgrade to enhance its physics capability over the next decades. The ATLAS Inner Detector will be replaced with silicon trackers, consisting of pixels and microstrip detectors, during the shutdown planned starting from the end of 2020 to be ready for the high-luminosity operation of LHC (HL-LHC) [1], [2]. The central part will consist of five layers of microstrip sensors, each with two silicon planes having a small stereo angle, to cover the radial volume 38 cm to 100 cm from the beam pipe. At 38 cm, the expected fluence is (5–9)$\times 10^{14}$ 1-MeV $n_{eq}/cm^2$ depending on the position along the beam for the target integrated luminosity of 3000 fb$^{-1}$, including a safety factor of two. The ATLAS radiation task force [3] estimates an annual dose of about 35 kGy at this radius and at $5\times 10^{34}$ cm$^{-2}$s$^{-1}$ (1 year=$10^7$ s), which gives average beam-on ionization dose of 13 Gy/h. Taking into account of the luminosity profile during the fill, about 20 Gy/h is the maximum instantaneous dose rate to examine.

The development of the Hamamatsu p-bulk sensors for the HL-LHC application started six years ago. We have carried out intensive radiation tolerance studies against protons and neutrons [4], [5], [6]. Main conclusion is that Hamamatsu sensors are applicable to the HL-LHC fluence. The charge collection of fully irradiated sensors is high enough to achieve sufficiently high signal-to-noise ratio of 15–20 at 500 V bias; the radiation-induced leakage current increase is similar to that of n-bulk sensors and is affordable; and the strip isolation is achievable.

While the FZ (float zone) wafers available to Hamamatsu Photonics show acceptable performance against proton and neutron irradiation, they exhibit instability at low dose. Fig. 1 shows I–V curves of a sample periodically measured under $^{60}$Co $\gamma$ irradiation. This sample showed no breakdown before irradiation. The breakdown voltage, or micro-discharge [7] onset voltage, dropped to 600 V then gradually recovered as accumulating the dose. Similar behavior is observed also for proton irradiation as shown in Fig. 2 [8]. Among many proton irradiated samples, one data sample for $^{60}$Co $\gamma$ irradiation is overlaid in the figure, where the horizontal is scaled in terms of the ionization dose due to protons. Since the curves agree with each other and the proton fluence is too small to induce bulk damage, the I–V instability should be attributed to the surface damage. We carried out a systematic study using $^{60}$Co $\gamma$ to characterize the effects and to understand the cause of the instability.

## 2. Samples and Measurements

The samples are ATLAS07[9] miniature sensors with outer dimensions of 10 mm $\times$ 10 mm $\times$ 0.32 mm having the strip length of 8 mm, see Fig. 3. The strip isolation is achieved by a common type p-stop having a nominal density of $4 \times 10^{12}$ ions/cm$^2$. The strip pitch is either 74.5 $\mu$m for Z3 and 100 $\mu$m for Z6 sensors. These sensors were used to investigate the pitch dependence of the stability. Two FZ p-type wafers, FZ1 and FZ2 [4], are available to Hamamatsu [10]. FZ2 wafers are standard quality while FZ1 have fewer defects than FZ1. Although the initial leakage current of FZ2 sensors is ten times larger than FZ1 sensors, the radiation tolerance to protons is similar to each other except at the low fluence [10].

The $^{60}$Co $\gamma$ irradiation tests were carried out at the JAEA(Takasaki) facility. The irradiation was made at room temperature. The samples were attached to the circuit boards

*Corresponding author
*Email address:* hara@hep.px.tsukuba.ac.jp (K. Hara)

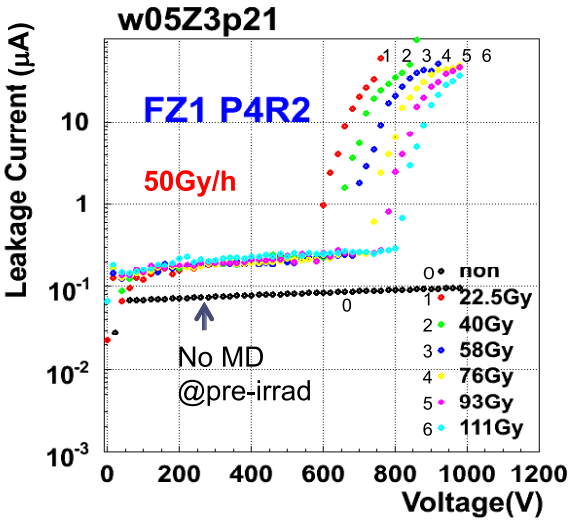


Figure 1: I–V curves of a sample measured periodically under 50 Gy/h $\gamma$ irradiation.

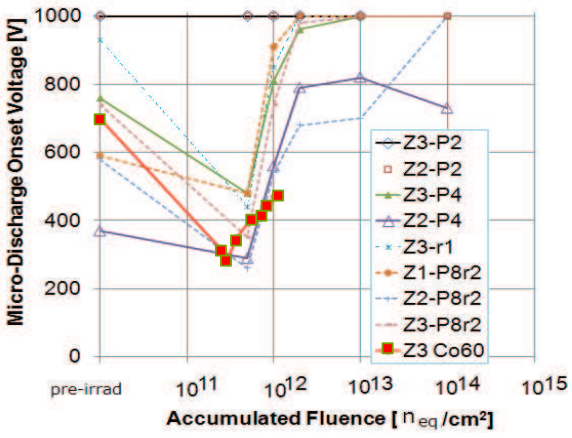


Figure 2: I–V curves of samples irradiated to protons. One sample (full squares) is from $\gamma$ irradiation where the ionization dose is used to scale the proton fluence.

where the biasing lines and a pair of DC pads at neighbor were extracted out by wire-bonding. The AC strips were not fixed to any potential in this measurement for ease of preparation. The bias voltages to the individual sensors, eight sensors maximum at a time, were provided using an iseg EHS8210n module that allows to bias up to 1000 V with a current reading resolution of 50 pA. The strip isolation was evaluated from the effective resistance measured between the DC pads at neighbor, the resistance being twice the bias resistors, *i.e.* $2 \times 1.5$ MΩ if the interstrip resistance is high enough compared to this value. As the strip isolation is degraded, the effective resistance becomes smaller than this value. The effective resistance was measured by applying ±5 V and reading the current with a Keithley 6517A.

Three kinds of measurements were performed:

- stability – The detector current was read out periodically at a 10 s interval typically while the sensor was irradiated at a fixed dose rate and at a fixed bias voltage, Vb_irrad. If the detector current exceeds the limit of 20 $\mu$A, the bias was lowered at a 10 V step.
- I-V – The detector I-V was measured periodically at a 20 min interval typically up to 1000 V or to the current limit while the sensor was irradiated at a fixed dose rate. The sensor bias other than in these measurements was set to a fixed value, Vb_irrad.
- isolation – The detector was irradiated at a fixed dose rate and at a fixed bias Vb_irrad. The isolation, the effective resistance, was measured periodically at a step of 50 V bias up to Vb_irrad.

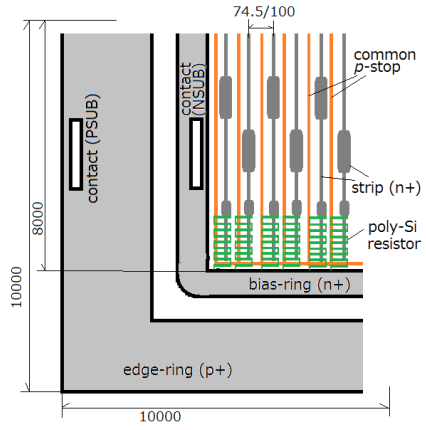


Figure 3: Layout of the sample sensor. The bias was applied through the two contacts made on the bias-ring and the edge-ring.

## 3. Results

### 3.1. Wafer dependence

Fig. 4 plots the evolution of micro-discharge (MD) onset voltages obtained from periodical I–V measurements. The irradiation was made with Vb_irrad of 200 V and at 200 Gy/h. The

curves are for four FZ1 and three FZ2 sensors, each showing a characteristic dependence. The onset voltage quickly dropped to 400–500 V (100 V) for FZ1 (FZ2) sensors from the initial onset of 900 V or above (450–600 V), then recovered gradually to their initial values after 400–500 Gy accumulated. Since the full depletion voltages are in the range from 180 to 200 V for these sensors, the FZ2 performance as observed is not acceptable. In the following, we concentrate mainly on the data for FZ1 sensors, and we revisit the FZ2 usability later.

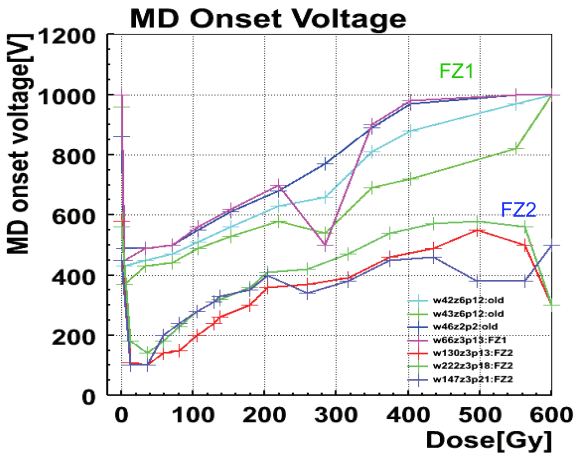


Figure 4: Micro-discharge onset voltage vs. accumulated dose, measured at 200 V bias and 200 Gy/h. The two clusters of the curves correspond to FZ1 and FZ2 wafers.

### 3.2. Dose rate dependence

The dose rate dependence of the MD onset voltages measured at Vb_irrad = 200 V is plotted in Fig. 5. The data are shown for two samples each at 5, 50 and 200 Gy/h. If there was no MD observed, the data point is plotted at 1000 V. As with lower radiation rate, the onset voltage degradation becomes smaller and the dose required for recovery becomes smaller.

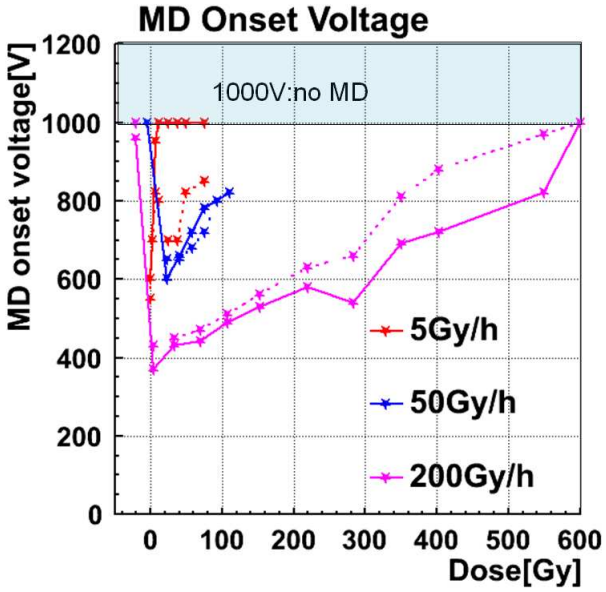


Figure 5: Dose rate dependence of MD onset voltage for FZ1, measured at 200 V bias. Two samples each of three dose rates, 5, 50 and 200 Gy/h.

### 3.3. Bias dependence

The previous data were taken at Vb_irrad = 200 V, since at higher biases we could not obtain meaningful data due to instability. Therefore we carried out a systematic measurement of sensor stability by measuring the current while keeping the bias at a fixed bias and dose rate.

The results are summarized in Fig. 6, the dose rate in horizontal and Vb_irrad in vertical. There are two numbers shown in each slot, Z3 at left and Z6 at right. The numbers with check marks are the doses in Gy up to which the sensor current was observed stable, while those with crosses are the doses where the sensor current reached the limit. The Z6 sensors show a stable range somewhat narrower than Z3 sensors, showing a strip pitch dependence of the stability. While both sensors are good to 100 Gy/h at 200 V bias, Z3 (Z6) sensors are good to 3 Gy/h (2 Gy/h) at 500 V which is the bias voltage foreseen at the HL-LHC. Note that only new sensors were used in this measurement and a certain stabilization is foreseen as the sensor accumulates the dose, as expected from Figs. 4 and 5.

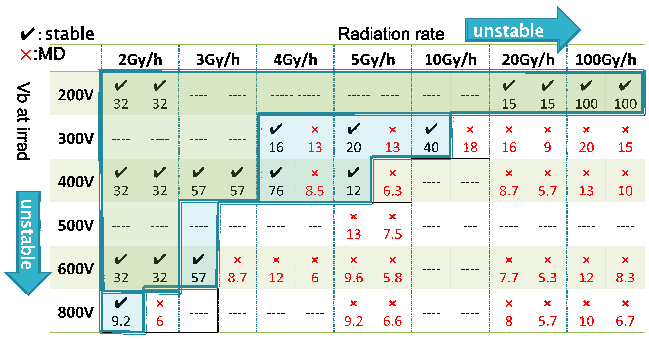


Figure 6: Stable (shaded) and unstable (unshaded) operation regions, measured at various bias voltages and dose rates. The samples are Z3 and Z6 sensors of FZ1 wafers which were never irradiated before.

### 3.4. Stabilization

Examples of sensor stabilization with accumulating dose are shown in Fig. 7. The MD onsets of four samples, two FZ1 and two FZ2, were measured first at 5 Gy/h and then twice at 50 Gy/h. The intervals between the series of measurements are as shown, 1 h between 1st and 2nd, and 0.5 h between 2nd and 3rd series. The MD disappeared in the 1st series, re-appeared in the 2nd, then no MD was observed in the 3rd series.

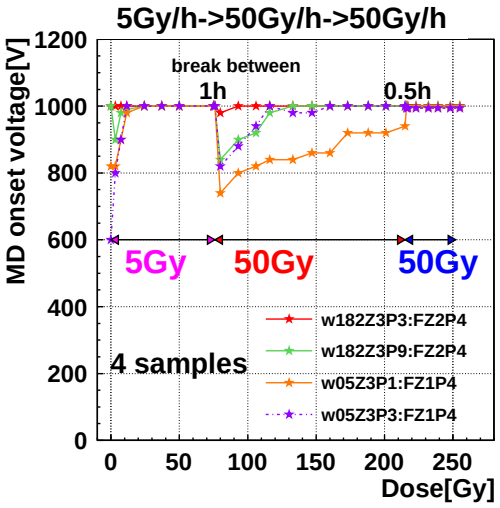


Figure 7: MD onset voltages of four samples measured first at 5 Gy/h and then twice at 50 Gy/h.

Fig. 8 shows the stability history of one sample measured at 20 Gy/h but increasing Vb_irrad in stepwise from 200 V, 500 V and to 700 V. The sensor became unstable at 500 V, but the sensor bias was tried reset periodically as far as the current is below the limit of 20 $\mu$A. Then this sensor became stable and kept stable throughout even at 700 V. Note that operation at 700 V and 20 Gy/h was not possible for new sensors, see Fig. 6, but this treatment makes it possible to operate the sensor in this condition. Operation at 700 V and 50 Gy/h was also made possible by similar treatment.

The observation of the sensor stabilization by irradiation was examined for eight samples which were irradiated three weeks ago. The sensors were kept refrigerated in this period. While four samples irradiated previously to 43 or 57 Gy showed instability in re-irradiation at 20 Gy/h and at 500 V bias, four other samples irradiated to 600 or 2000 Gy were stable in re-irradiation at the same conditions. A critical dose of a few 100 Gy to maintain the sensor stability is consistent with the doses in Figs. 4 and 5 where similar amount of dose is required for the sensor recovery.

### 3.5. Reason of instability

The breakdown sensors were examined with an infrared-sensitive camera[11] to investigate the location of MD points. The back-thinned cooled CCD camera, HPK C4880, can sensitively image the heat created in the process of avalanche multiplication associated in micro-discharge.

Fig. 9 shows four rows of AC pads and an enlarged view showing hot-spots observed at the AC pad corners. Some other examined samples show similar images. The electric field at the AC pad corners is strongest, collecting largest amount of signal current.

The dose rate dependence and weakness for the wider pitch sensor can be understood from larger current to be collected to the corner. The bias dependence of the stability is interpreted as the development of avalanche becomes larger with the bias. Since the initial leakage current of FZ2 is about 10 times larger than that of FZ1, the FZ2 sensors are more sensitive in avalanche development. Note that no sample showed hot spots at the DC pad and p-stop, where the curvature of the electrode corners are similar to that of the AC pad. Therefore the floating insulator should be another key to explain the observed phenomenon. We note that the AC aluminum electrode is extended by 3 $\mu$m over the $n^+$ electrode. The insulator layer traps some of the holes created from developing avalanches and accumulating the radiation dose. Electrons are attracted to these trapped holes and accumulated on the silicon surface, which effectively widens the electrode and relaxes the field concentration especially at the corner of the electrodes. Since the field distribution is dependent on whether the aluminum electrode is floating or wirebonded to the amplifier, the time-constant of the relaxation may be modified in the real configuration where amplifiers are connected.

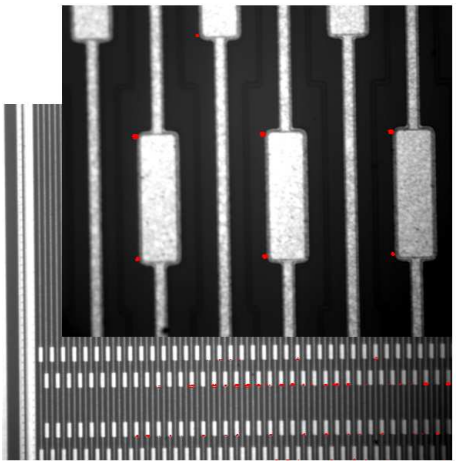

Figure 9: Hot spots observed at AC pad corners. The AC pad is 60 $\mu$m wide and 200 $\mu$m long.

### 3.6. Isolation degradation

The strip isolation degradation during irradiation is reported in [10]. We repeated similar measurement for various Vb_irrad settings. The results are shown in Fig. 10, where the isolation-achieved voltage is plotted for two samples set at each of Vb_irrad of 200, 300, 400 and 500 V. Here, we define the isolation achieved voltage as the bias at which the effective resistance is equal to the bias resistance. This definition is arbitrarily, since we found the effective resistance increased and reached the initial value in a few minutes if we keep the bias at Vb_irrad. This suggests that the isolation degradation is partially caused by lowering the bias to perform the measurement, although radiation induced effects are indeed present. In all the

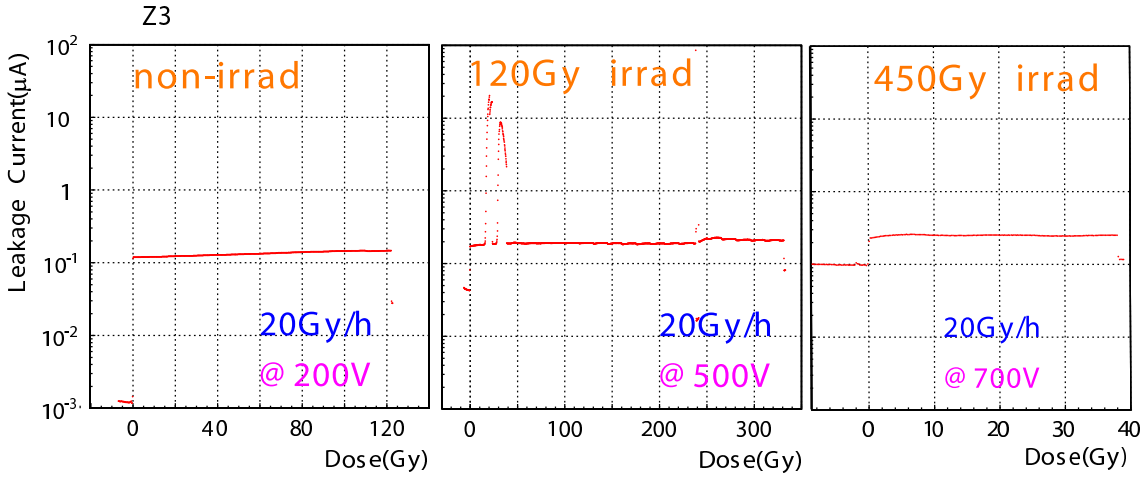


Figure 8: Example of a sensor stability irradiated at 20 Gy/h. The bias was increased in three irradiation periods.

cases the isolation achieved voltages stay within Vb_irrad and no practical problem should exist.

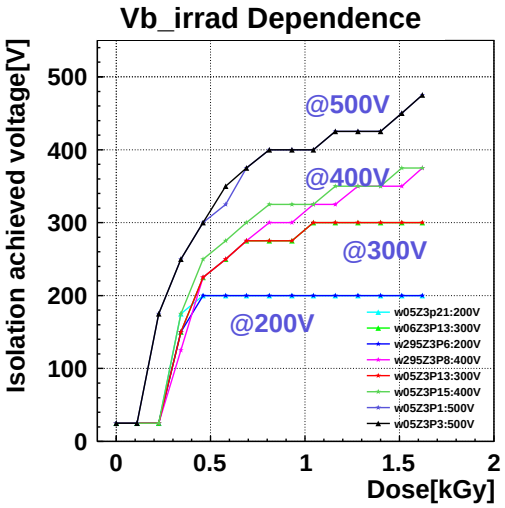


Figure 10: Evolution of isolation achieved voltage for various Vb_irrad settings.

## 4. Conclusions

We have evaluated the stability of Hamamatsu p-bulk sensors by irradiating them with $^{60}$Co $\gamma$'s at rates expected at the HL-LHC. The sensors are stable at rates exceeding 100 Gy/h if they are operated at 200 V bias. The sensor becomes more unstable at higher bias and higher dose rate. New sensors that were never irradiated before are relatively easier to become unstable but repeating irradiation can make the sensor stable allowing operation at 700 V bias even at 50–70 Gy/h.

The initial instability can be attributed to the large amount of charges collected to the AC pad corners, where the electric field is maximum and micro-discharge is easier to develop especially at higher bias voltages. After accumulating 100–200 Gy, charges trapped in oxide layers act to reduce the electric field, enhancing the stability of the sensors.

The instability of Hamamatsu p-bulk microstrip sensors observed at low ionization dose are characterized. Together with the study made with protons and neutrons to full expected fluence, FZ1 wafer is usable to the HL-LHC. FZ2 wafer which is less stable at low ionization doses should also become usable by repeating irradiation, while further study is required to conclude the usability.

## References

[1] S. Diez Cornell, in: this issue.
[2] A. Clark, in: this issue.
[3] S. Baranov, et al., Radiation background task force, 2004. http://bosman.home.cern.ch/bosman/Radiation_maps.html.
[4] K. Hara, et al., IEEE TNS 56-2 (2009) 468.
[5] K. Hara, et al., Nuclear Instruments and Methods A636 (2011) S83.
[6] S. Lindgren, et al., Nuclear Instruments and Methods A636 (2011) S111.
[7] T. Ohsugi, et al., Nuclear Instruments and Methods A383 (1996).
[8] M. Yamada, et al., Surface damages in p-bulk silicon microstrip sensors, 2009. Presented at TIPP09 Tsukuba conference, Mar. 12-17.
[9] Y. Unno, et al., Nuclear Instruments and Methods A636 (2011) S24.
[10] K. Hara, et al., IEEE NSS CR N04-5 (2008).
[11] T. Kuwano, et al., Nuclear Instruments and Methods A579 (2007) 782.